

TESS planets in known radial velocity cold Jupiter systems: Hot super Earth occurrence is enhanced by cold Jupiters

QUANYI LIU (刘权毅) ,¹ WEI ZHU (祝伟) ,¹ TIANJUN GAN (干天君) ,² AND FEI DAI (戴飞) ,³

¹Department of Astronomy, Tsinghua University, Beijing 100084, China

²Department of Astronomy, Westlake University, Hangzhou 310030, Zhejiang Province, China

³Institute for Astronomy, University of Hawai'i, 2680 Woodlawn Drive, Honolulu, HI 96822, USA

ABSTRACT

The correlation between inner super-Earths (SEs) and outer cold Jupiters (CJs) provides an important constraint on the formation and dynamical evolution of planetary systems. Previous studies have suggested a positive connection between these two populations, particularly around metal-rich stars, and proposed that nearly all CJ-hosting stars may also harbor inner SEs. In this work, we use TESS transit to investigate the occurrence of hot SEs in systems with known CJs detected by radial velocity (RV). Out of a statistical sample of 132 CJ systems, we identify five transiting hot super-Earths ($1\text{--}4R_{\oplus}$, $P < 10$ d) around four stars, including one new candidate (TOI-6965.01) around HD 50554. To enable statistical analysis, we first validate the two candidates around HD 50554 using TESS photometry, archival RV measurements, and Gaia astrometry. After accounting for detection sensitivity and geometric transit probability, we find that the presence of CJs enhances the occurrence rate of hot super-Earths by a factor of $8.1_{-3.2}^{+4.3}$ relative to field stars, with the case of no enhancement being ruled out at 99.9% confidence level. Taking into account the average multiplicity of hot SEs, we find that about 87% of CJ systems host at least one hot SE. Our results provide strong supporting evidence for a positive SE–CJ correlation. We also briefly explore the correlation around metal-poor hosts and for specific sub-populations (e.g., warm super Earths or cold super Jupiters).

Keywords: Exoplanet systems (484), Exoplanet detection methods (489), Astrostatistics (1882)

1. INTRODUCTION

The connection between close-in small planets—most notably super-Earths (SEs), defined as planets with masses or radii between those of Earth and Neptune—and cold Jupiters (CJs), which are gas giants located beyond ~ 1 au, has attracted increasing attention in exoplanet studies. This connection is closely related to the search for true Solar System analogs (e.g., Zhu & Dong 2021; Fernandes et al. 2025). It also provides important constraints on the physical processes that govern the formation and evolution of planetary systems (e.g., Bitsch et al. 2020; Schlecker et al. 2021; Guo & Kokubo 2023; Best et al. 2024; Huang et al. 2025; Danti et al. 2025).

Corresponding author: Wei Zhu
 weizhu@tsinghua.edu.cn

From the observational perspective, Zhu & Wu (2018) and Bryan et al. (2019) first reported that the occurrence rate of CJs in systems hosting SEs, denoted as $P(\text{CJ|SE})$, is about 30%, which is about three times higher than that in field stars without regard to inner small planets. This suggests a positive correlation between the two planet populations. Following these early works, some later studies also found a positive correlation (e.g. Herman et al. 2019; Rosenthal et al. 2022; Van Zandt et al. 2025), while some others reported an indifferent or even negative correlation (e.g. Bonomo et al. 2023). Such discrepancies can be largely reconciled when considering the metallicity and mass dependences of the cold Jupiter occurrence rate (Zhu 2024; Bryan & Lee 2025), and the correlation appears to be significant at least around metal-rich Sun-like stars (Bryan & Lee 2024; Bonomo et al. 2025). For other stellar types and bulk metallicities, the available dataset is not large enough to tell the difference between positive and no correlation.

For practical reasons, the majority of the existing studies have focused on measuring $P(\text{CJ}|\text{SE})$, whereas the inverted conditional rate, $P(\text{SE}|\text{CJ})$, namely the occurrence of SEs in systems hosting CJs, has rarely been directly constrained. This inverted conditional rate is more directly related to theories that attempt to explain the SE–CJ connection (e.g., Schlecker et al. 2021; Bitsch & Izidoro 2023; Danti et al. 2025). By applying Bayes’ theorem, Zhu & Wu (2018) and Bryan et al. (2019) inferred that nearly all CJs should have at least one inner SE companion. However, this predicted high conditional probability carries substantial uncertainty due to Bayesian error propagation. Two studies have attempted to constrain $P(\text{SE}|\text{CJ})$ directly. In searching for long-period (> 2 yr) transiting giant planet candidates in the *Kepler* data, Herman et al. (2019) found five out of their 15 long-period giant candidates hosted inner small companions. With the assumption that the inner and the outer systems are not highly misaligned ($\lesssim 4^\circ$), they reported that $\sim 90\%$ of systems hosting long-period giants also contain inner small planets (see also Masuda et al. 2020). In addition to the unknown mutual inclinations, another issue with the Herman et al. (2019) approach is that not all of their giant planets in size are actually giant planets in mass, as some other similar objects have been known to have rather small masses (e.g., HIP 41378 f Santerne et al. 2019). Another direct measurement of the inverted conditional rate is by Rosenthal et al. (2022). Using a radial-velocity (RV) sample from the California Legacy Survey (CLS, Rosenthal et al. 2021), Rosenthal et al. (2022) found that the occurrence rate of inner (< 1 au) low-mass ($2\text{--}30 M_\oplus$) planets increases from 27% to 42% in the presence of an outer ($0.23\text{--}10$ au) massive ($> 0.1 M_J$) planet. Their definitions of inner and outer planets differ from the commonly adopted ones, making it hard to have a direct comparison. Additionally, the use of a pure (and possibly biased) RV sample limits the sensitivities to only relatively massive planets, whereas the lower-mass but more abundant planets cannot be probed.

RV surveys have undoubtedly been very successful in delivering hundreds of exoplanet detections and constraining the distribution of exoplanets, especially the relatively massive ones (e.g., Cumming et al. 2008; Mayor et al. 2011; Howard et al. 2011). However, the current RV surveys are typically insufficient in detecting Earth-mass or even super Earth-mass planets at relatively wide orbits. For example, a $5 M_\oplus$ planet at 50-day orbit around a Solar-mass star only produces a RV semi-amplitude of ~ 1 m/s, which is detectable only by hyper stable instruments on quiet stars with aggressive observing strategies. Detection of low-mass planets in

the presence of massive giant planets is even harder (e.g., Anglada-Escudé et al. 2010). The large-amplitude, long-period RV signal induced by the outer giant can dominate the RV time series, making it challenging to disentangle the low-amplitude signals of inner small planets. In comparison, space-based transit surveys have been proven to be more efficient in detecting small planets, and these detections are largely unaffected by the presence of additional bodies in the system (e.g., Lissauer et al. 2011; Fabrycky et al. 2014).

The Transiting Exoplanet Survey Satellite (TESS, Ricker et al. 2015) is designed to conduct an all-sky transit survey of bright, nearby stars, providing an ideal data set for detecting short-period transiting super Earths. Owing to its high photometric precision and continuous monitoring over ~ 27 -day sectors, TESS is particularly sensitive to planets with orbital periods of days to weeks, a regime that is challenging for RV surveys alone. Notably, the first exoplanet discovered by TESS, π Mensae c (Huang et al. 2018; Gandolfi et al. 2018), is a short-period super Earth orbiting a Sun-like star that also hosts a known long-period cold Jupiter (HD 39091 b, Jones et al. 2002). Another similar system was also found later by Teske et al. (2020). In both cases, the inner super Earths were not detected by RV alone prior to the TESS transit, even though intensive RV measurements had been conducted.

Motivated by these archetypal systems, we attempt to investigate the occurrence of transiting super Earths in systems with known RV cold Jupiters using TESS photometry. Compared to previous studies based on either transit samples or RV surveys alone, our approach combines the strengths of both techniques: the well-characterized RV sample provides a clean census of outer giant planets, while TESS enables a uniform and sensitive search for short-period SEs around the same host stars. This strategy allows us to directly constrain the probability of having inner super-Earths, especially the low-mass ones, in cold-Jupiter systems, while explicitly accounting for transit and detection completeness, thereby offering a more robust observational test of the SE-CJ correlation.

This paper is organized as follows: In Section 2, we describe our sample of systems with RV CJ; in Section 3, we describe our pipeline to search for transiting SEs in TESS data and quantify the detection completeness; in Section 4, we confirm the planetary nature of two new transiting SE candidates around HD 50554; in Section 5, we estimate the occurrence rate of SE in our sample; finally in Section 6, we summarize our findings and discuss the implications of our results.

2. THE RV COLD JUPITER SAMPLE

The sample used in this work is drawn from the NASA Exoplanet Archive (NEA, Christiansen et al. 2025; retrieved on Nov. 16, 2025). We select cold Jupiters satisfying the following criteria:

1. The host has no known stellar companions, as indicated by the NEA label `sy_snum`. This is to remove binaries or multi-star systems as they may complicate the transit search and analysis.
2. The host is a Sun-like main-sequence star, defined to have a stellar mass in the range $0.6 M_{\odot} < M_{\star} < 1.4 M_{\odot}$ and a stellar radius below $2 R_{\odot}$. For a few entries that do not have values for stellar mass or radius, we manually checked their status based on the discovery papers. Focusing on Sun-like main-sequence hosts allow us to have direct comparisons with previous studies.
3. The discovery method for the planet is “Radial Velocity”.
4. The planet is qualified as a cold Jupiter, defined to have a minimum mass in the range $0.3 M_{\mathrm{J}} < M_{\mathrm{p}} \sin i < 20 M_{\mathrm{J}}$, orbital period $P > 300$ d, and semi-major axis $a < 10$ au.
5. The planet is not discovered as part of follow-up observations of transiting systems. This is achieved by excluding systems with any of the following keywords in the name: WASP, HAT, Kepler, TOI, TIC, K2, KELT, and CoRoT.
6. The planet has no hot ($P < 10$ days) or warm ($10 \text{ d} < P < 300 \text{ d}$) Jupiter companions ($m \sin i > 0.3 M_{\mathrm{J}}$). Similar to the previous criterion, the cold Jupiters beyond HJ or WJ orbits may have been detected through targeted follow-up rather than blind searches.
7. The host star has TESS SPOC light curves, and there are no bright ($\Delta m_G < 5$ mag) contaminants within the TESS aperture according to Gaia DR3 (Gaia Collaboration et al. 2023). The existence of such nearby bright stars would complicate the validation of any potential transit signals.

Our sample does not include several systems known to host both transiting SEs and CJs, most notably 55 Cancri and HD 191939. The 55 Cancri system has a stellar companion and hosts a warm Jupiter with an orbital period of 14 days (Butler et al. 1997). HD 191939 is excluded because its cold Jupiter was discovered only after the discovery of the inner transiting planets, and it also hosts a warm Jupiter with an orbital period of 102 days (Badenas-Agusti et al. 2020; Lubin et al. 2022).

Table 1. Cold Jupiters catalog of the sample.

System name	TIC	N_{pl}	TESS sectors
HD 100777	49427341	1	6, 7, 87
HD 102843	79290210	1	4, 31
HD 10442	380908091	1	7, 34
HD 105779	347713631	1	12
HD 106252	397558558	1	10, 37
HD 10647	229137615	1	29
...

NOTE—This table is published in its entirety in the machine-readable format. Only a portion of it is shown here for guidance regarding its form and content.

NOTE—Here N_{pl} denotes the number of known planets in the system, as reported in NEA.

Finally, our sample contains 132 systems hosting 149 CJs. The host name is provided in Table 1, and these systems are shown in Figure 1. Distributions of the stellar masses and TESS magnitudes of these systems are shown in Figure 2. The majority of the stars are truly solar-like with masses between 0.8 – $1.2 M_{\odot}$. These stars are relatively bright, with the overwhelming majority having TESS magnitude < 8 , whereas, for comparisons, TOIs found from the TESS primary mission typically have magnitudes in the range 8–10 (Guerrero et al. 2021). This bias towards bright stars is understandable, as almost all of the stars in our sample are targets of RV surveys, which preferentially select bright Sun-like stars (Wright et al. 2012).

A cross-match with the TESS Object of Interest (TOI, Guerrero et al. 2021) table shows that five out of 132 systems contain transiting super Earths, including three with confirmed planets: HD 39091 (π Mensae, Huang et al. 2018; Gandolfi et al. 2018), HD 219134 (Gillon et al. 2017; Motalebi et al. 2015),¹ and HD 86226 (Teske et al. 2020). There are additionally two systems hosting TESS planet candidates: HD 50554 (TOI-6965.01 and 6965.02) and HIP 54597 (TOI-6709.01). Almost all of the TESS transiting planets in these systems fall within the hot super-Earth (HSE for short hereafter) regime, with orbital periods shorter than 10 days and radii between 1 – $4 R_{\oplus}$, except for one candidate, TOI-6965.02 in

¹ Unlike the HD 191939 system, the cold Jupiter in HD 219134 was first detected, and the transiting signal of the inner small planet was detected later (Vogt et al. 2015; Motalebi et al. 2015; Gillon et al. 2017).

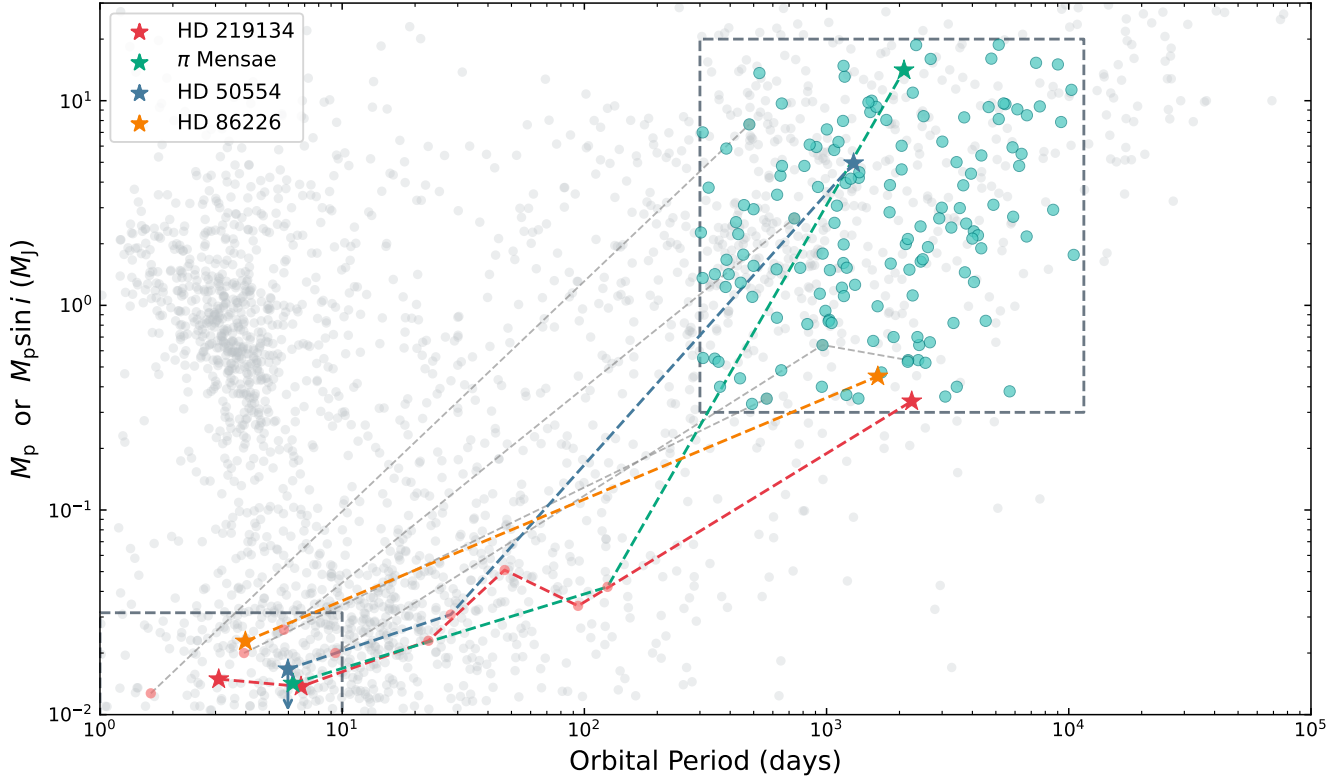


Figure 1. Planet mass (or minimum mass) as a function of orbital period for planetary systems hosting cold Jupiters. Gray points represent the full population of confirmed exoplanets from the NASA Exoplanet Archive. The dashed box outlines the parameter space adopted for CJs and HSEs in this work. Colored stars denote systems in our sample that host both a CJ and at least one inner SE detected by TESS: HD 219134, π Mensae, HD 50554, and HD 86226. Cyan circles indicate CJs in our RV-selected sample without detected transiting inner SEs. Other HSEs detected via RV, along with planets in their systems, are marked by pink circles. Planets belonging to the same system are connected by dashed lines.

HD 50554. In the next section, we will carry out our own transit search and quantify its detection efficiency.

3. TESS TRANSIT ANALYSIS

3.1. *Transit search*

To guarantee the consistency of the statistical analysis and the completeness correction, we build our own pipeline to search for the SE transit signals in TESS data. For each target in our sample, we first retrieve the TESS Presearch Data Conditioning Simple Aperture Photometry (PDCSAP) light curve, processed by the Science Processing Operations Center (SPOC; Jenkins et al. 2016) pipeline, using the `lightkurve` package (Lightkurve Collaboration et al. 2018). The data are accessed as of November 25, 2025. We detrend the light curves using the `biweight` method with a window length of 0.3 d, and clip outliers that are more than three times the median absolute deviation (MAD) from the median value within the same window length.

Then we conduct the box least square (BLS; Kovács et al. 2002) search in order to identify the transit signals. The BLS search is performed on a two-dimensional grid, with 10,000 and 100 equally spaced values along orbital period between 1-10 days and transit duration between 0.01-0.3 days, respectively. We adopt the threshold-crossing event (TCE) criteria used in the TESS pipeline (Guerrero et al. 2021), which define that a periodic signal is considered detected if it satisfies both (1) a BLS peak significance > 9 , and (2) a signal-to-pink-noise ratio $S/N_{\text{pink}} > 9$. The BLS peak significance is computed as the height of the maximum BLS peak relative to the noise floor of the periodogram, defined as the median BLS power within a ± 0.3 -day window around the peak. The period and transit duration values corresponding to the highest BLS significance are used to calculate S/N_{pink} , which is defined as

$$S/N_{\text{pink}} = \frac{\delta}{\sqrt{(\sigma_w^2/n_d) + (\sigma_r^2/N_{\text{tr}})}}. \quad (1)$$

Here δ is the transit depth, and σ_w and σ_r are the white and red noises of the light curve, respectively. Quanti-

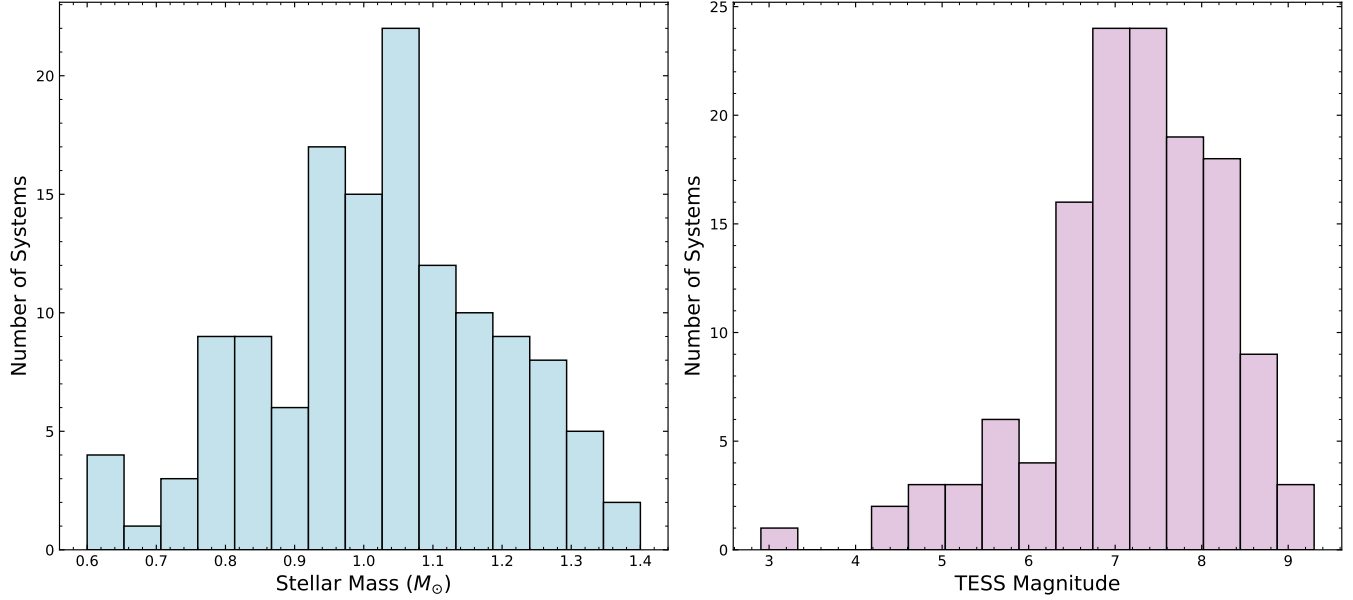


Figure 2. The distribution of the cold Jupiter host stars in our sample. Left: The histogram of stellar mass. Right: The histogram of TESS magnitude.

ties n_d and N_{tr} are the number of in-transit points and the number of transits, respectively (Pont et al. 2006; Hartman & Bakos 2016). We follow the procedure of Kunimoto et al. (2025) in computing each of those parameters in Equation (1).

Out of the 132 systems with RV cold Jupiters, our pipeline detects five transit candidates, as listed in Table 2. Four of them correspond to TESS-confirmed planets: π Men c, HD 86226 c, and HD 219134 b and c. The fifth one is the TESS candidate TOI-6965.01 around HD 50554. Two other TESS transit candidates that were mentioned in Section 2, namely TOI-6965.02 around HD 50554 and TOI-6709.01 around HIP 54597, are not detected by our pipeline. For TOI-6965.02, its orbital period of 28 days exceeds the period range explored by our pipeline, and TOI-6709.01 has a low transit S/N that did not pass our detection criteria. Since these two candidates are not detected by our pipeline, we do not include them in our transiting SE sample. Given the unconfirmed status of TOI-6965.01, we will first validate its planetary nature in Section 4 before proceeding to the sample statistics. The second candidate in the same system, TOI-6965.02, is also validated, even though it will not be included in the statistical analysis.

Besides the transit signals, our pipeline also identifies three systems—HD 165131, HD 70642, and HD 80883—whose light curves exhibit periodic signals that formally satisfy our detection criteria. However, inspection of the phase-folded light curves reveals sinusoidal variations rather than transit-like features, indicating that these signals are not of planetary transit origin. Such

Table 2. TESS transiting super Earths in the RV cold Jupiter systems of our sample.

Planet name	TOI	Period (days)	$R_p (R_\oplus)$	Ref.
HD 39091 c (π Men c)	144.01	6.26790 (46)	2.04 (5)	1
HD 86226 c	652.01	3.98442 (18)	2.16 (8)	2
HD 219134 b	1469.01	3.0935 (3)	1.61 (9)	3
HD 219134 c	1469.02	6.76458 (33)	1.511 (47)	4
HD 50554 c	6965.01	5.969362 (20)	1.31 (6)	5

NOTE—References: (1) Huang et al. (2018), (2) Teske et al. (2020), (3) Motalebi et al. (2015), (4) Gillon et al. (2017), (5) This work

sinusoidal trends were not removed by our detrending procedure because their periods (~ 0.2 days) are shorter than the 0.3-day window used for detrending. We can in principle remove these three systems from our sample because of the false signals from the sinusoidal variations. However, these targets have otherwise low photometric noise levels, and our injection–recovery tests show that the injected transit signals are unaffected by the sinusoidal photometric behavior and thus detectable nevertheless. Given this and the fact that these systems are rare among our sample, we therefore retain these three targets in our final sample.

3.2. Detection efficiency calculation

We quantify the detection efficiency of our search pipeline through an injection—recovery experiment. For systems with known transiting planets, we remove their transit signals based on the best-fit parameters from NEA, and we manually check this step and make sure that no peak in the BLS periodogram has significance above nine.

For each target, we inject 200 synthetic transit signals into the raw light curve. Similar to Gan et al. (2023), planetary radii are randomly drawn from 1–4 R_{\oplus} , orbital periods are sampled from a log-uniform distribution between 1–10 days, and impact parameters are randomly drawn with $b \leq 0.9$. The epoch of the first transit is randomly assigned between the start of the observations, t_{begin} , and $t_{\text{begin}} + P$. For simplicity, we adopt fixed quadratic limb-darkening coefficients $(u_1, u_2) = (0.3, 0.3)$ for all injections. Synthetic transit models are generated using the analytic formalism of Mandel & Agol (2002), as implemented in the `batman` package (Kreidberg 2015). We correct for the dilution effect by modifying the injected radius ratio R_p/R_{\star} to $(R_p/R_{\star})/\sqrt{1+A_D}$ (Gan et al. 2023; Espinoza et al. 2019), where A_D is the contamination ratio reported by TIC v8 (Stassun et al. 2019). These models are then injected into the raw light curves and passed through our full transit-search pipeline to evaluate the recovery efficiency.

During the recovery stage, we largely follow the search procedure described in Section 3.1, including the detrending and detection process, except for one minor revision. In estimating S/N_{pink} , we adopt directly the value of the injected orbital period rather than performing the grid search. This obviously speeds up the process, and it also avoids the occasional situations where the most significant BLS peak may be mistakenly attributed to harmonics of the injected period or the sinusoidal variations (for the three systems discussed in Section 3.1).

The injection–recovery experiment is done for all target stars in our sample, and the detection sensitivity is defined as the ratio between recovered signals and all injected signals. The sensitivity map is derived on a 5×4 grid in the orbital period–radius plane, as is shown in the left panel of Figure 3. No validations of the injected signals were performed in our experiment, as our sample is quite clean and exempt from any severe false positives. The only exception is the three targets with sinusoidal variations, but their effect has been mitigated in the signal evaluation step. Figure 3 shows that TESS achieves a typical detection sensitivity of roughly $\sim 50\%$ for planets with radii between 1–4 R_{\oplus} and orbital peri-

ods between 1–10 days around the RV targets with cold Jupiters.

The geometric transit probability is evaluated as

$$p_{\text{tr}} = 0.9 \frac{R_{\star}}{a} = 0.9 R_{\star} \left(\frac{GM_{\star}P^2}{4\pi^2} \right)^{-1/3}. \quad (2)$$

The factor of 0.9 comes from considering only transit planets with $b < 0.9$ in this study. Taking the transit probability into account, the search completeness map is shown in the right panel of Figure 3. The above evaluation has assumed an isotropic distribution for the orbital inclination of the transiting super Earths, which we argue remains a reasonable assumption even though these systems have RV cold Jupiter detections. On one hand, the orbital inclinations of the RV cold Jupiters may deviate from an ideal isotropic distribution because of the RV detection bias. On the other hand, the mutual inclinations between the inner small planets and the outer giants, although small on average (Masuda et al. 2020), depend on the planet multiplicity and can be significant for systems with only one or two planets (Herman et al. 2019). Detailed analyses of systems like π Mensae indeed confirm the presence of large mutual inclinations (Xuan & Wyatt 2020; De Rosa et al. 2020; Damasso et al. 2020). More discussions on the latter point will be given in Section 6.2.3.

4. VALIDATION OF TWO SUPER EARTHS AROUND HD 50554

4.1. TESS observations & light curve modeling

HD 50554 is a Sun-like star with TESS magnitude of 6.31 (see Table 3 for more details). TESS observed this star at a 20-second cadence in Sectors 44, 45, 71, and 72. The target pixel file (TPF) and photometric aperture used in Sector 72 are shown in Figure 4, which is made via `tpfplotter` (Aller et al. 2020). According to Gaia DR3, the second brightest star in the aperture is still about 8 mag fainter than the target, so we can ignore the light contamination from nearby stars. Data acquisition and pre-processing are performed following the procedures given in Section 3.1. We confirmed the 5.97 d signal with a BLS significance of 10.8 and a S/N_{pink} of 13.4, both above the thresholds to be claimed as a detection. However, our pipeline is not suitable for searching for the second signal with 28.07 d period, as the detrending with a 0.3-day window may suppress the corresponding transit signal. To detrend the light curve while preserving the transit signals, we first mask out the transit events based on the NEA parameter values and then fit a Gaussian process (GP) model with the Matern-3/2 kernel using the `celerite`

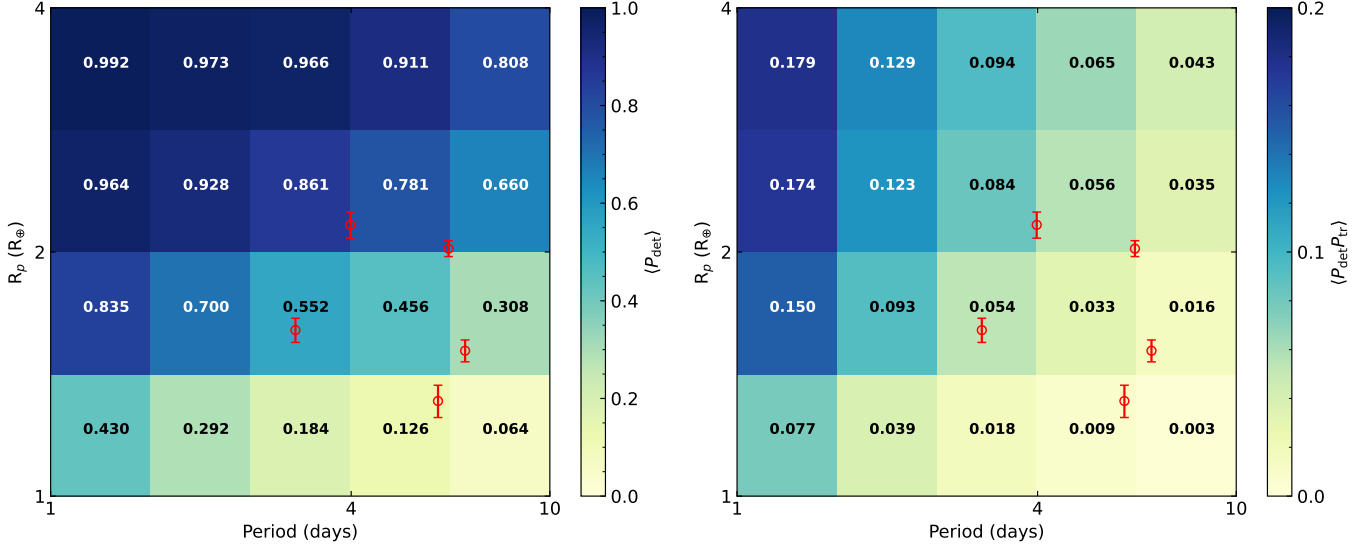


Figure 3. The average detection sensitivity map (left panel) and the full completeness (i.e., detection sensitivity & transit probability) map (right panel) as a function of orbital period and planet radius. The number in each cell represents the average detection probability across all 132 targets. The red circles with error bars indicate the five HSEs detected by our pipeline.

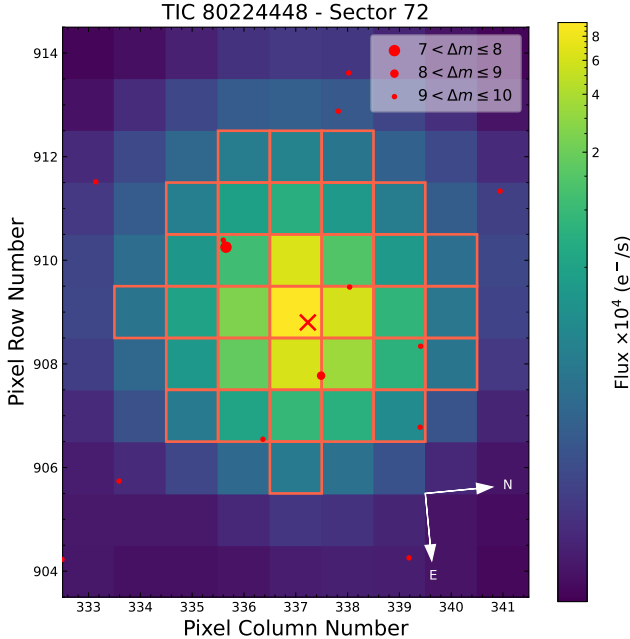


Figure 4. TESS TPF image of HD 50554 (TIC 80224448) observed in Sector 72. Orange squares outline the photometric apertures. The red cross marks the nominal position of the target star. Red dots denote nearby Gaia sources, and the sizes of dots reflect their magnitude difference compared to the HD 50554.

package (Foreman-Mackey et al. 2017). The flattened light curve is shown in the top panel of Figure 5.

We model the TESS light curve using the Mandel & Agol (2002) model as implemented in `Batman` (Kreidberg 2015). Over nearly 800 days covered by the four sec-

tors, there are 16 transits of the inner candidate (TOI-6965.01) and four transits of the outer candidate (TOI-6965.02). We select only data with a 1-day length centered on the expected transit mid-point for light curve modeling. A quadratic limb-darkening law is adopted, and the re-parameterization into q_1 and q_2 according to Kipping (2013) is used. We use the Markov chain Monte Carlo (MCMC) method as implemented in `emcee` of Foreman-Mackey et al. (2013) to sample the posterior distributions of the model parameters. The phase-folded light curves of two candidates are shown in the lower panels of Figure 5. The median values and $1-\sigma$ uncertainties of the model parameters determined from the posterior distributions are summarized in Table 3.

According to our model, the two transiting planet candidates around HD 50554 have radii of $1.31 \pm 0.06 R_{\oplus}$ and $1.41^{+0.14}_{-0.09} R_{\oplus}$ and orbital periods of ~ 6 and ~ 28 days, respectively. Therefore, they both fall below the radius valley and are thus likely rocky with no thick envelopes (Fulton et al. 2017; Owen & Wu 2017).

4.2. Mass constraints from archival RV

The super Jupiter HD 50554 b, with minimum mass $\sim 4 M_{\oplus}$ and semi-major axis ~ 2.3 au around HD 50554 was discovered independently by Fischer et al. (2002) and Perrier et al. (2003). Since then, the star has been continuously observed for more than two decades, but no other RV signals have been detected (e.g., Xiao et al. 2023). Given the estimated masses of $\sim 2 M_{\oplus}$ and $\sim 3 M_{\oplus}$ from the Chen & Kipping (2017) mass-radius relation, the two transiting planets produce RV semi-amplitudes of 0.7 and 0.6 m/s, respectively. It is

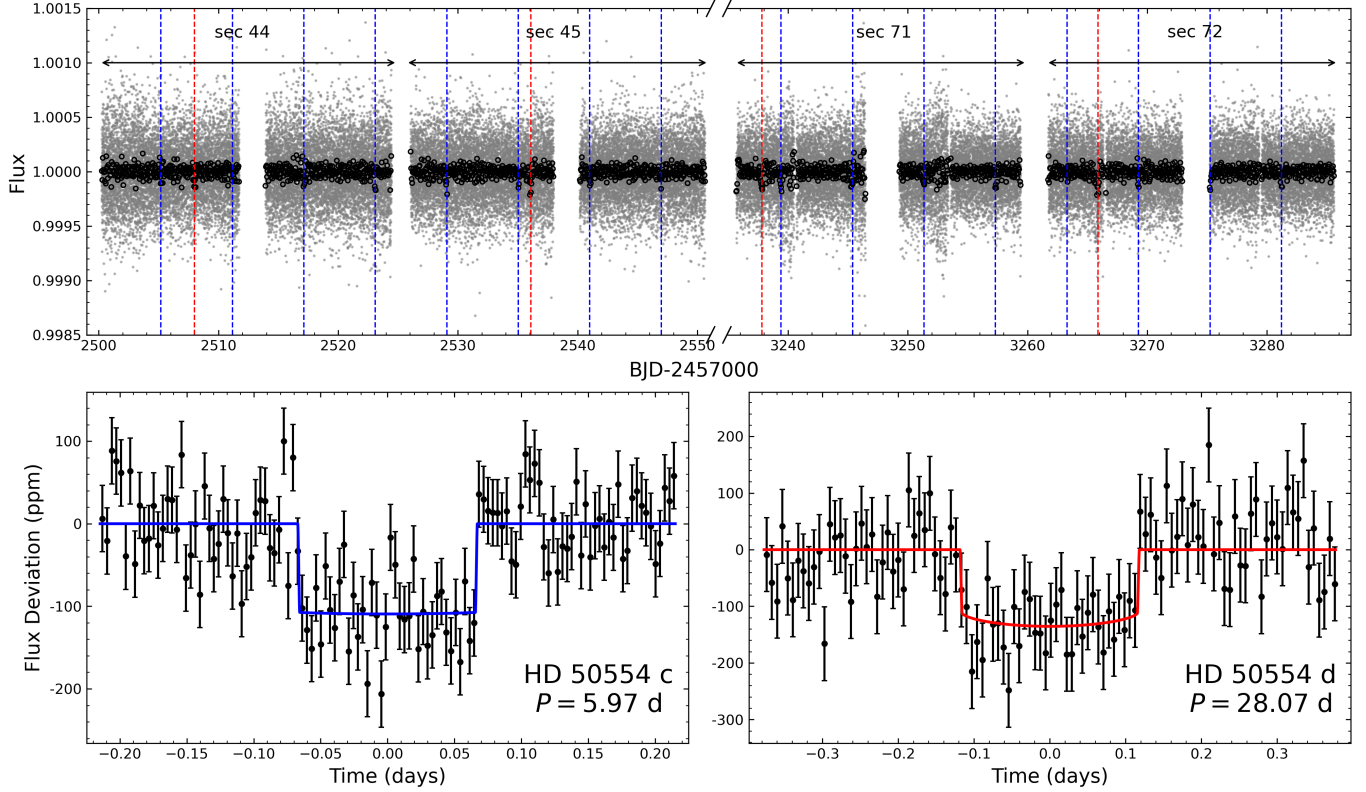


Figure 5. The TESS light curves of HD 50554. The top panel shows the flattened TESS light curves from Sectors 44, 45, 71, and 72. Grey points indicate short-cadence data with 2-minute sampling, and black points are 1-hour averages for visualization. Blue and red dashed lines mark the predicted mid-transit times of HD 50554 c (TOI-6965.01) and d (TOI-6965.02), respectively. The bottom panels show the phase-folded light curve, along with the best-fitting model of HD 50554 c (left) and HD 50554 d (right). The black dots represent 5-minute averages in the left and 10-minute averages in the right.

therefore not a surprise that these planets have not been detected.

We nevertheless attempt to place limits on the masses of the two planet candidates. In this analysis, we include RV measurements from the California Legacy Survey (CLS, Rosenthal et al. 2021), which collected a total of 157 observations from Keck/HIRES, APF/Levy, and Lick/Hamilton, and archival measurements from ELODIE (Perrier et al. 2003), as presented in Figure 6. The RV modeling is done through the `radvel` package (Fulton et al. 2018). We first identify the model parameters corresponding to HD 50554 b and then subtract its signal from the RV data. We then fit the residuals to constrain the semi-amplitudes of the two inner candidates, assuming circular orbits for both planets. In this step, we have imposed Gaussian priors on the orbital periods and mid-transit epochs from the transit fit. These RV data yield 95% upper limits of 5.3 and $10.4 M_{\oplus}$ for the 6-day and 28-day planets, respectively.

4.3. Transit signal validation

We have searched for odd–even variations and searched for secondary eclipses in the TESS light curve, and both candidates pass these vettings. Together with the non-detection of the RV signals at the known orbital periods, these add further confidence that the transit signals are indeed produced by low-mass planets around the target star. Other false positive scenarios are also ruled out:

- HD 50554 has no stellar companion(s) that could explain the transit signals. HD 50554 b has a measured true mass of $\sim 6 M_{\mathrm{J}}$, based on a joint modeling to the Gaia and Hipparcos astrometric measurements (Xiao et al. 2023). Apart from HD 50554 b, there is no other periodic signal in the RV data, and the lack of a linear trend in the RV residuals rules out any massive objects within ~ 30 au, which, combined with the known distance of HD 50554, corresponds to an angular separation of $\sim 1''$. The presence of a stellar companion at wider separations is ruled out by Gaia DR3 (Gaia Collaboration et al. 2023).

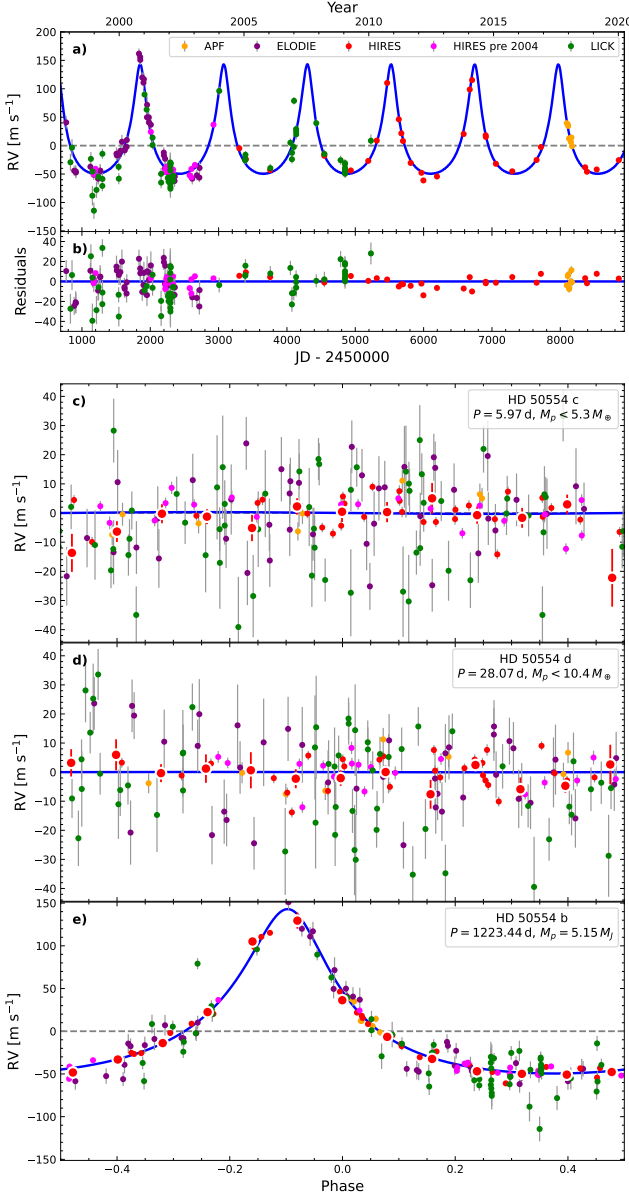


Figure 6. Radial-velocity analysis of the HD 50554 system plotted by `radvel`. (a-b) Current public RV time-series and residuals of the full three-planet model. (c-e) Phase-folded RV signals for planets c, d, and b, respectively. The blue curves show the corresponding best-fit orbital models.

- The transit events cannot be explained by background stars unassociated with HD 50554. As shown in Figure 4, there are no stars of comparable brightness ($\Delta m < 5$) within the TESS aperture. In order to explain the 100 ppm transit signals on the 6.3 mag target, a nearby star brighter than ~ 16 mag is required. According to Gaia DR3, four stars pass this threshold within the TESS aperture, and the brightest of them have $m_{\text{TESS}} = 14$. Here we have converted the Gaia G

Table 3. Stellar and planetary parameters of the HD 50554 system

Stellar Parameters	Value	Reference
TIC ID	80224448	1
TOI ID	6965	
TESS mag	6.31	1
$M_*(M_\odot)$	1.04 (5)	2
$R_*(R_\odot)$	1.146 (26)	2
[Fe/H]	-0.02 (6)	2
T_{eff} (K)	5968 (96)	2
Distance (pc)	31.070 (23)	3
Planet Parameters	Planet c	Planet d
T_c (TBJD)	2505.1917 (20)	2508.005 (9)
P (days)	5.969362 (20)	28.06940 (40)
R_p/R_*	0.01045 (41)	$0.0113^{+0.0011}_{-0.0007}$
R_p (R_\oplus)	1.31 (6)	$1.41^{+0.14}_{-0.09}$
b	$0.49^{+0.29}_{-0.33}$	0.50 (35)
a/R_*	$12.3^{+1.6}_{-3.4}$	31^{+5}_{-12}
a (au)	$0.066^{+0.009}_{-0.018}$	$0.168^{+0.028}_{-0.065}$
$T_{14,\text{tr}}$ (hr) ^a	$3.30^{+0.14}_{-0.09}$	$6.21^{+0.64}_{-0.44}$
$T_{12,\text{tr}}$ (hr) ^a	$0.12^{+0.13}_{-0.08}$	$0.73^{+0.59}_{-0.43}$
M_p (M_\oplus)	$< 5.3^b$	$< 10.4^b$

NOTE—References: (1) Stassun et al. (2019), (2) Rosenthal et al. (2021), (3) Gaia Collaboration et al. (2023)

^aFrom trapezoidal transit models.

^bThe 95% upper limit of planetary masses.

magnitudes to TESS magnitudes using the relations given in Stassun et al. (2019). For such faint stars to account for the transit signals, the eclipsing events would need to be intrinsically deep, with an estimated eclipsing depth of

$$\delta_{\text{EB}} = \delta \left(1 + 10^{0.4 \Delta m_{\text{TESS}}} \right). \quad (3)$$

For the faint star with $m_{\text{TESS}} = 14$, the eclipsing depths without dilution are 14% and 16% for the two candidate signals, respectively. Such deep eclipses would yield V-shaped light curves with large ingress-to-total-duration ratios ($T_{12}/T_{14} \gtrsim 0.28$ and $\gtrsim 0.30$, respectively). Such scenarios are effectively ruled out by our transit constraints (see Table 3). In principle, there could be other stars that are unbound to HD 50554 and yet unresolved by Gaia. However, considering the angular resolution of Gaia ($\sim 0.7''$, Gaia Collaboration et al.

2023) and the low spatial density of stars around HD 50554, the probability for such a scenario to occur is extremely small ($\sim 4 \times 10^{-4}$).

5. SUPER EARTH OCCURRENCE RATE ENHANCED BY THE PRESENCE OF COLD JUPITERS

Our sample contains 132 Sun-like stars hosting RV-detected cold Jupiters, among which four contain in total five transiting super Earths with orbital periods below 10 d. These numbers strongly suggest that the occurrence of hot super Earths is enhanced by the presence of cold Jupiters, as is explained below.

In the absence of any correlation between HSEs and CJs, the expected number of transiting HSEs should follows their intrinsic occurrence rate, which can be estimated as

$$\bar{N}_{\text{HSE}} = N_{\star} \sum_{i,j} \eta_{\text{HSE},ij} \cdot p_{\text{tr},ij} \cdot p_{\text{det},ij}. \quad (4)$$

Here $N_{\star} = 132$ is the total number of stars in the sample, η_{HSE} denotes the HSE occurrence rate in the period vs. radius plane, p_{tr} is the geometric transit probability (Equation 2), and p_{det} is the pipeline detection efficiency map (left panel in Figure 3). The summation is performed over both orbital period (index i) and planetary radius (index j) directions. Adopting the HSE occurrence rate distribution given in Figure 3 of Zhu & Dong (2021), which was derived from the Kepler sample, we obtain $\bar{N}_{\text{HSE}} = 0.58$, which is substantially smaller than the number of actual detections ($N_{\text{HSE}} = 5$).

To quantify the impact of CJ on the occurrence rate of HSE, we define an enhancement factor f

$$f \equiv \frac{\eta(\text{HSE}|\text{CJ})}{\eta(\text{HSE})}. \quad (5)$$

With a Poisson likelihood assumed for the number of HSE detections and a flat prior adopted on f , the posterior distribution of the enhancement factor f given N_{HSE} and \bar{N}_{HSE} follows a Gamma distribution with a shape parameter $N_{\text{HSE}} + 1$ and a rate parameter \bar{N}_{HSE}

$$P(f|N_{\text{HSE}}, \bar{N}_{\text{HSE}}) = \frac{\bar{N}_{\text{HSE}}^{N_{\text{HSE}}+1}}{\Gamma(N_{\text{HSE}}+1)} f^{N_{\text{HSE}}} e^{-f\bar{N}_{\text{HSE}}}. \quad (6)$$

With $\bar{N}_{\text{HSE}} = 0.58$ and $N_{\text{HSE}} = 5$, the enhancement factor is constrained to be $f = 8.1_{-3.2}^{+4.3}$ (68% confidence interval). The posterior distribution of the enhancement is shown in Figure 7. The probability of $f \leq 1$ is only 0.1%, which implies we can safely rule out that the presence of CJs will suppress the existence of HSE at high

statistical significance ($p < 0.001$). This result is insensitive to the adopted HSE occurrence rate map. For example, adopting the HSE occurrence rates from Figure 6 of Petigura et al. (2018), we obtain $\bar{N}_{\text{HSE}} = 0.41$ and an enhancement factor of $f = 10.7_{-4.2}^{+5.7}$. These consistent results suggest that the presence of CJs does enhance the occurrence of HSEs by a factor of a few.

The above enhancement factor is insensitive to our definitions of CJ and/or WJ. If we apply different definitions of CJ and WJ in our sample selection, the sample size is changed slightly, and the number of systems hosting transiting HSE remains the same. The enhancement factor derived under these different definitions therefore remain largely unchanged, as is shown in Table 4.

With the known value of $\eta(\text{HSE}) = 0.135$ from Zhu & Dong (2021), we constrain the occurrence rate of HSE around Sun-like stars with at least one cold Jupiter,

$$\eta(\text{HSE}|\text{CJ}) = 1.09_{-0.43}^{+0.58}, \quad (7)$$

and $\eta(\text{HSE}|\text{CJ}) = 1.23_{-0.48}^{+0.66}$ using $\eta(\text{HSE}) = 0.115$ from Petigura et al. 2018.

In the above estimate, we have assumed that the HSE occurrence rate of our selected TESS Sun-like stars is the same as that from Kepler. The only issue that may make this assumption less valid is the different metallicity distributions between our RV cold Jupiter sample and the sample of either Zhu & Dong (2021) or Petigura et al. (2018). The RV cold Jupiter sample is on average more metal-rich (see Figure 8 for example), whereas the Kepler Sun-like star sample has an average metallicity around Solar value (Dong et al. 2014). However, the occurrence rate of HSE is known to correlate with stellar metallicity only weakly. If we adopt the metallicity dependence of HSE from Petigura et al. (2018), $\eta(\text{HSE}) \propto 10^{\beta[\text{Fe}/\text{H}]}$ with $\beta \approx 0.6$, and a metallicity difference of $\Delta[\text{Fe}/\text{H}] \approx 0.2$ dex, then the occurrence rate of HSE is lifted by a factor of ~ 1.3 . This difference due to metallicity effect is small compared to the statistical uncertainty of the derived conditional occurrence rates.

We can go a step further to derive the fraction of Sun-like stars with at least one HSE given that there is already at least one cold Jupiter, $P(\text{HSE}|\text{CJ})$. The distinction between this and $\eta(\text{HSE}|\text{CJ})$ is in the planet multiplicity. Super Earths are frequently found in multi-planet systems (Lissauer et al. 2011; Fabrycky et al. 2014), and each system may contain on average ~ 3 such planets within 1 au (Zhu et al. 2018). Although the average multiplicity of hot super Earths is not known, we can take the observed average multiplicity of our sample ($5/4 = 1.25$) as an appropriate estimate. Then we have

$$P(\text{HSE}|\text{CJ}) \approx 87\%. \quad (8)$$

Table 4. Sample sizes and enhancement factor under different selection criteria. The first case is our fiducial criterion as listed in Section 2, where CJ is defined as $0.3 < M_p \sin i < 20 M_J$, $P > 300$ days and $a < 10$ au, WJ is defined as $0.3 < M_p \sin i < 20 M_J$, $P < 300$ days. The brackets in the subsequent columns show the definitions that are different from the fiducial criterion.

Selection criterion	Sample size	Enhancement factor
CJ ($0.3 < M_p \sin i < 20 M_J$) systems without WJ ($P < 300$ days)	4/132	$8.1^{+4.3}_{-3.2}$
CJ ($0.3 < M_p \sin i < 13 M_J$) systems without WJ ($P < 300$ days)	4/124	$8.6^{+4.6}_{-3.4}$
CJ ($0.3 < M_p \sin i < 20 M_J$) systems without WJ ($P < 100$ days)	4/141	$7.6^{+5.8}_{-4.2}$

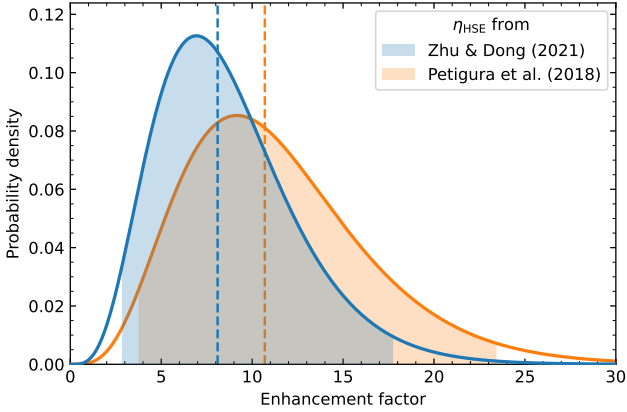


Figure 7. Posterior distributions of the enhancement factor of the occurrence rate of hot SE in the presence of CJ. The two distributions shown in different colors are derived using the occurrence rates of HSEs from Zhu & Dong (2021) and Petigura et al. (2018), respectively. The median values are indicated by the vertical dashed lines, and the 95% confidence interval about the median is indicated by the shaded region.

That is, about 87% of Sun-like stars with cold Jupiters also host hot super Earths.

6. SUMMARY & DISCUSSION

6.1. Summary

This work studies the correlation between cold Jupiters and hot super Earths. We uniformly selected 132 systems with Sun-like hosts and at least one known cold Jupiter detected via RV. To avoid the potential biases associated with hot and warm Jupiters, cold Jupiters with such inner friends were excluded from the sample. We then systematically and uniformly searched for transiting signals around these 132 stars in the TESS data and identified five transiting hot super Earths around four stars, including one transiting candidate (TOI-6965.01) with a period of 6 d around HD 50554.

Combining TESS photometry, archival RV measurements, and Gaia astrometry, we were able to confirm the planetary nature of the two transiting candidates around HD 50554, even though the outer one with a period of 28 d was not in our statistical sample. The available RV measurements were only able to constrain the

masses of these two super Earths with radii of $1.3 M_{\oplus}$ and $1.4 M_{\oplus}$ to $< 5.3 M_{\oplus}$ and $10.4 M_{\oplus}$, respectively.

Our statistical sample of 132 stars yields five hot super Earths from four stars. From these we report an enhancement factor of $8.1^{+4.3}_{-3.2}$ in the occurrence rate of hot super Earths by the presence of cold Jupiters. Taking into account the average multiplicity of hot super Earths, we find that the fraction of Sun-like stars with hot super Earths given that there is already at least one cold Jupiter is about 87%. These numbers indicate a strong correlation between the hot super Earth and cold Jupiter populations.

Below we discuss what our results imply in a broader context.

6.2. Implications to the super Earth–cold Jupiter connection

6.2.1. Impact of stellar metallicity

Recent studies have confirmed that the stellar metallicity plays a role in the correlation. While the positive correlation has been reported around metal-rich stars (Zhu 2024; Bryan & Lee 2024; Bonomo et al. 2025), no consensus has been reached about the metal-poor end. This is probably because those studies all focused on the conditional probability of cold Jupiters given super Earths, $P(\text{CJ|SE})$. As cold Jupiter occurrence correlates strongly with host star metallicity (e.g., Santos et al. 2001, 2004; Fischer & Valenti 2005), the absolute rate of $P(\text{CJ})$ is no more than a few percent if one is limited to sub-solar metallicities, and the value of $P(\text{CJ|SE})$ is probably $\lesssim 10\%$ even if the correlation remains as strong as it is in the metal-rich side. To measure such a small value with high significance and thus confirm (or not) the correlation in the metal-poor side thus requires a large sample size, exceeding what is available at the moment (e.g., Bryan & Lee 2024; Bonomo et al. 2025).

The derivation of the converted conditional rate, namely $P(\text{SE|CJ})$, is less affected by stellar metallicity, because the occurrence of super Earths correlates much more weakly, if at all, with stellar metallicity (e.g., Buchhave et al. 2014; Petigura et al. 2018; Zhu 2019). This approach faces its own challenges, however, as it requires to detect the low-mass super Earths in the presence of cold Jupiters. Although dedicated searches may be able

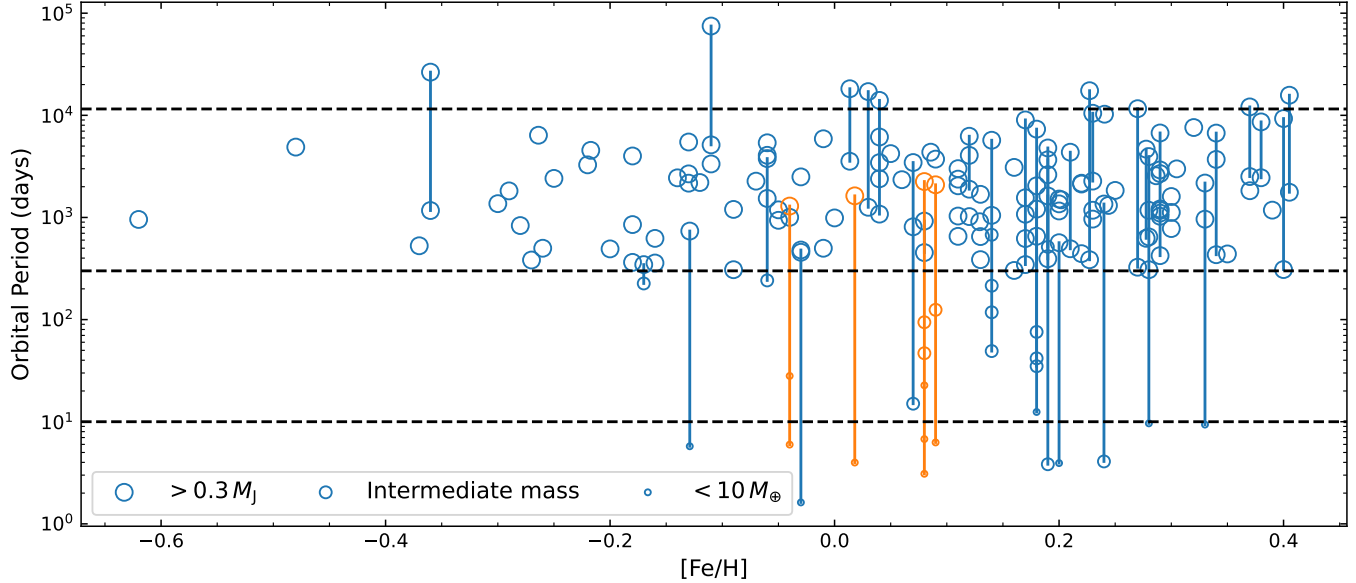


Figure 8. The planetary systems with RV CJs in our sample as a function of host star metallicity. The four systems with transiting HSE discovered by TESS are marked in orange.

to make it (Delisle et al. 2025), this requirement is generally difficult for RV method. One way to navigate the challenge would be to combine different detection methods, as is done here. Our sample consists of stars that have cold Jupiter detections from RV, and then we search for inner super Earths with transit.

If we set the distinction between metal-rich and metal-poor at solar value and exclude one system that has no reliable metallicity measurement, then there are 43 metal-poor and 88 metal-rich CJ systems, and the number of systems with transiting hot super Earths for the two subsamples are one and three, respectively. See Figure 8 for an illustration of our sample along the metallicity dimension. The ratios, $1/43$ vs. $3/88$, are quite compatible with each other,² and they are both substantially higher, in the statistical sense, than the expected ratio (~ 0.006) under the assumption of null correlation (see Section 5). Therefore, our results suggest that the super Earth–cold Jupiter correlation remains strong in the metal-poor regime. If we define metal-poor as with $[\text{Fe}/\text{H}] < 0.05$ and metal-rich as with $[\text{Fe}/\text{H}] > 0.05$ to avoid the potential complication of metallicity uncertainties, then we have 34 and 80 in the metal-poor and metal-rich subsamples, and the numbers of hot super Earth detections in TESS are zero and two, respectively. These numbers are still consistent with a positive correlation between super Earths and cold Jupiters across

different stellar metallicities, although the alternative explanation is not ruled out. Future studies based on larger samples, in particular by making use of the Gaia giant planet detections (Espinoza-Retamal et al. 2023), should provide more conclusive results on this matter.

6.2.2. How about warm super Earths?

We choose to study the correlation between cold Jupiters and hot super Earths because of the sensitivity limitation of TESS. For super Earths with longer periods (10–300 d), namely warm super Earths, the transit probability significantly reduces, and the observing strategy of TESS was not able to produce homogeneous period coverage. Nevertheless, at least one of our targets, HD 50554, does contain a transiting warm super Earth (see Section 4). Additionally, as shown in Figure 1, some targets in our sample also host warm super Earths that were detected by RV, and HD 39091 (π Mensae) might host a $\sim 13 M_\oplus$ planet at 125-day orbit (Hatzes et al. 2022). Therefore, (at least some) warm super Earths can get along with cold Jupiters.

Do warm super Earths also correlate with cold Jupiters, just like their hot siblings? From a theoretical perspective, warm super Earths can be easily perturbed by the eccentric outer giants during the dynamical evolution of the system (e.g., Schlecker et al. 2021; Bitsch & Izidoro 2023), and the occurrence of warm super Earths does seem to show a negative correlation with increasing metallicity (Petigura et al. 2018). These would suggest that the occurrence of warm super Earths may be suppressed by the presence of cold Jupiters. However, a suppressed occurrence rate of warm super Earths does

² We note that HIP 54597 has $[\text{Fe}/\text{H}] \approx -0.22$ (Frensch et al. 2023; Philipot et al. 2023), although the transiting hot super Earth around it, TOI-6709.01, does not meet our detection threshold.

not necessarily mean a suppressed occurrence rate of warm super Earth systems, and it is the rate of systems that matters more to the connection with cold Jupiters (Zhu 2019). Unfortunately, this latter quantity cannot be constrained with the currently available data, so we are not yet able to answer the question that is posted in the beginning of this paragraph.

6.2.3. *Cold super Jupiter vs. cold Saturn*

A recent work by Lefèvre-Forján & Mulders (2025) claimed that the presence of inner low-mass planets ($< 0.1 M_J$) preferentially correlates with outer giants of Saturn-mass ($0.1\text{--}1.5 M_J$) rather than super-Jupiter ($> 1.5 M_J$), based on a re-analysis of the pure RV sample of CLS. While there are several differences in the definitions of close-in planets and distant giants as well as whether restricting to Sun-like stars (FGK dwarfs, as in the present work) or mixing all stellar types and evolution stages (as in Lefèvre-Forján & Mulders 2025), here we focus on the main conclusion of that study, namely that super Jupiters do not correlate with close-in low-mass planets.

As shown in Figure 1, the masses (to be more accurate, projected masses) of the cold Jupiters with inner transiting hot super Earths in our sample span almost the entire allowed mass range, from $\approx 0.34 M_J$ (HD 219134 h) to $\approx 14 M_J$ (HD 39091 b, or π Mensae b). The cold Jupiter in our newly confirmed TESS transiting system, HD 50554 b, also joins the super-Jupiter category that is defined by Lefèvre-Forján & Mulders (2025), whereas the cold Jupiter in the fourth system (HD 86226 b) would be classified as Saturn-mass. Because the four systems straddle two ends of the cold Jupiter mass, any statistical analysis would be very sensitive to how one divides super-Jupiter vs. Saturn-mass. Nevertheless, the existence of systems like π Mensae and HD 50554 does seem to contradict the claim of Lefèvre-Forján & Mul-

ders (2025). In other words, the most massive giant planets can be accompanied by inner super Earths.

The discovery process of the π Mensae and HD 50554 systems also shed light on the limitations of pure RV samples. In both systems, the inner super-Earths were not detected by RV first, despite that both stars had received intensive RV observations. Yet π Mensae c and HD 50554 c and d have relatively short periods, rendering them relatively high RV amplitudes. The bulk of the super Earth population have even small RV signals, and disentangling them from the much stronger signals of cold Jupiters—especially eccentric super Jupiters—will be very challenging.

Another interesting feature to note before we conclude this section is that two systems hosting both RV super Jupiters and transiting super Earths are both dynamically hot, with the super Jupiters exhibiting large eccentricities and significant mutual inclinations with respect to the inner super Earths: HD 39091 b has an eccentricity of ~ 0.6 and an inclination of $\sim 54^\circ$, implying a mutual inclination of $\gtrsim 36^\circ$ with respect to π Men c (Feng et al. 2022; see also Xuan & Wyatt 2020; De Rosa et al. 2020; Damasso et al. 2020); HD 50554 b has an eccentricity of ~ 0.5 and an inclination of $\sim 61^\circ$, corresponding to a mutual inclination of $\gtrsim 30^\circ$ relative to the inner transiting planets (Xiao et al. 2023). The two systems containing Saturn-mass cold giants and inner transiting super Earths do seem to be dynamically colder, as is evidenced by the small eccentricities of both HD 219134 h (~ 0.06 , e.g. Vogt et al. 2015) and HD 86226 b (~ 0.06 , e.g. Teske et al. 2020). It is unclear whether there is really a dichotomy or a rather smooth distribution that connects the two quite different architectures.

This work is supported by the National Natural Science Foundation of China (grant No. 12173021 & 12133005). We also acknowledge the Tsinghua Astrophysics High-Performance Computing platform for providing computational and data storage resources.

REFERENCES

Aller, A., Lillo-Box, J., Jones, D., Miranda, L. F., & Barceló Forteza, S. 2020, A&A, 635, A128, doi: [10.1051/0004-6361/201937118](https://doi.org/10.1051/0004-6361/201937118)

Anglada-Escudé, G., López-Morales, M., & Chambers, J. E. 2010, ApJ, 709, 168, doi: [10.1088/0004-637X/709/1/168](https://doi.org/10.1088/0004-637X/709/1/168)

Badenas-Agusti, M., Günther, M. N., Daylan, T., et al. 2020, AJ, 160, 113, doi: [10.3847/1538-3881/aba0b5](https://doi.org/10.3847/1538-3881/aba0b5)

Best, M., Sefilian, A. A., & Petrovich, C. 2024, ApJ, 960, 89, doi: [10.3847/1538-4357/ad0965](https://doi.org/10.3847/1538-4357/ad0965)

Bitsch, B., & Izidoro, A. 2023, A&A, 674, A178, doi: [10.1051/0004-6361/202245040](https://doi.org/10.1051/0004-6361/202245040)

Bitsch, B., Trifonov, T., & Izidoro, A. 2020, A&A, 643, A66, doi: [10.1051/0004-6361/202038856](https://doi.org/10.1051/0004-6361/202038856)

Bonomo, A. S., Naponiello, L., Pezzetta, E., et al. 2025, A&A, 700, A126, doi: [10.1051/0004-6361/202452523](https://doi.org/10.1051/0004-6361/202452523)

Bonomo, A. S., Dumusque, X., Massa, A., et al. 2023, A&A, 677, A33, doi: [10.1051/0004-6361/202346211](https://doi.org/10.1051/0004-6361/202346211)

Bryan, M. L., Knutson, H. A., Lee, E. J., et al. 2019, AJ, 157, 52, doi: [10.3847/1538-3881/aaf57f](https://doi.org/10.3847/1538-3881/aaf57f)

Bryan, M. L., & Lee, E. J. 2024, ApJL, 968, L25, doi: [10.3847/2041-8213/ad5013](https://doi.org/10.3847/2041-8213/ad5013)

—. 2025, ApJL, 982, L7, doi: [10.3847/2041-8213/adb0bd](https://doi.org/10.3847/2041-8213/adb0bd)

Buchhave, L. A., Bizzarro, M., Latham, D. W., et al. 2014, Nature, 509, 593, doi: [10.1038/nature13254](https://doi.org/10.1038/nature13254)

Butler, R. P., Marcy, G. W., Williams, E., Hauser, H., & Shirts, P. 1997, ApJL, 474, L115, doi: [10.1086/310444](https://doi.org/10.1086/310444)

Chen, J., & Kipping, D. 2017, ApJ, 834, 17, doi: [10.3847/1538-4357/834/1/17](https://doi.org/10.3847/1538-4357/834/1/17)

Christiansen, J. L., McElroy, D. L., Harbut, M., et al. 2025, PSJ, 6, 186, doi: [10.3847/PSJ/ade3c2](https://doi.org/10.3847/PSJ/ade3c2)

Cumming, A., Butler, R. P., Marcy, G. W., et al. 2008, PASP, 120, 531, doi: [10.1086/588487](https://doi.org/10.1086/588487)

Damasso, M., Sozzetti, A., Lovis, C., et al. 2020, A&A, 642, A31, doi: [10.1051/0004-6361/202038416](https://doi.org/10.1051/0004-6361/202038416)

Danti, C., Lambrechts, M., & Lorek, S. 2025, A&A, 700, A132, doi: [10.1051/0004-6361/202555095](https://doi.org/10.1051/0004-6361/202555095)

De Rosa, R. J., Dawson, R., & Nielsen, E. L. 2020, A&A, 640, A73, doi: [10.1051/0004-6361/202038496](https://doi.org/10.1051/0004-6361/202038496)

Delisle, J.-B., Faria, J. P., Ségransan, D., et al. 2025, A&A, 703, A78, doi: [10.1051/0004-6361/202555445](https://doi.org/10.1051/0004-6361/202555445)

Dong, S., Zheng, Z., Zhu, Z., et al. 2014, ApJL, 789, L3, doi: [10.1088/2041-8205/789/1/L3](https://doi.org/10.1088/2041-8205/789/1/L3)

Espinoza, N., Kossakowski, D., & Brahm, R. 2019, MNRAS, 490, 2262, doi: [10.1093/mnras/stz2688](https://doi.org/10.1093/mnras/stz2688)

Espinoza-Retamal, J. I., Zhu, W., & Petrovich, C. 2023, AJ, 166, 231, doi: [10.3847/1538-3881/ad00b9](https://doi.org/10.3847/1538-3881/ad00b9)

Fabrycky, D. C., Lissauer, J. J., Ragozzine, D., et al. 2014, ApJ, 790, 146, doi: [10.1088/0004-637X/790/2/146](https://doi.org/10.1088/0004-637X/790/2/146)

Feng, F., Butler, R. P., Vogt, S. S., et al. 2022, ApJS, 262, 21, doi: [10.3847/1538-4365/ac7e57](https://doi.org/10.3847/1538-4365/ac7e57)

Fernandes, R. B., Johnson, S., Bergsten, G. J., et al. 2025, PASP, 137, 121001, doi: [10.1088/1538-3873/ae215a](https://doi.org/10.1088/1538-3873/ae215a)

Fischer, D. A., Marcy, G. W., Butler, R. P., et al. 2002, PASP, 114, 529, doi: [10.1086/341677](https://doi.org/10.1086/341677)

Fischer, D. A., & Valenti, J. 2005, ApJ, 622, 1102, doi: [10.1086/428383](https://doi.org/10.1086/428383)

Foreman-Mackey, D., Agol, E., Ambikasaran, S., & Angus, R. 2017, AJ, 154, 220, doi: [10.3847/1538-3881/aa9332](https://doi.org/10.3847/1538-3881/aa9332)

Foreman-Mackey, D., Hogg, D. W., Lang, D., & Goodman, J. 2013, Publications of the Astronomical Society of the Pacific, 125, 306, doi: [10.1086/670067](https://doi.org/10.1086/670067)

Frensch, Y. G. C., Lo Curto, G., Bouchy, F., et al. 2023, A&A, 675, A173, doi: [10.1051/0004-6361/202346203](https://doi.org/10.1051/0004-6361/202346203)

Fulton, B. J., Petigura, E. A., Blunt, S., & Sinukoff, E. 2018, PASP, 130, 044504, doi: [10.1088/1538-3873/aaaaaa8](https://doi.org/10.1088/1538-3873/aaaaaa8)

Fulton, B. J., Petigura, E. A., Howard, A. W., et al. 2017, AJ, 154, 109, doi: [10.3847/1538-3881/aa80eb](https://doi.org/10.3847/1538-3881/aa80eb)

Gaia Collaboration, Vallenari, A., Brown, A. G. A., et al. 2023, A&A, 674, A1, doi: [10.1051/0004-6361/202243940](https://doi.org/10.1051/0004-6361/202243940)

Gan, T., Wang, S. X., Wang, S., et al. 2023, AJ, 165, 17, doi: [10.3847/1538-3881/ac9b12](https://doi.org/10.3847/1538-3881/ac9b12)

Gandolfi, D., Barragán, O., Livingston, J. H., et al. 2018, A&A, 619, L10, doi: [10.1051/0004-6361/201834289](https://doi.org/10.1051/0004-6361/201834289)

Gillon, M., Demory, B.-O., Van Grootel, V., et al. 2017, Nature Astronomy, 1, 0056, doi: [10.1038/s41550-017-0056](https://doi.org/10.1038/s41550-017-0056)

Guerrero, N. M., Seager, S., Huang, C. X., et al. 2021, ApJS, 254, 39, doi: [10.3847/1538-4365/abef1](https://doi.org/10.3847/1538-4365/abef1)

Guo, K., & Kokubo, E. 2023, ApJ, 955, 109, doi: [10.3847/1538-4357/acf31d](https://doi.org/10.3847/1538-4357/acf31d)

Hartman, J. D., & Bakos, G. Á. 2016, Astronomy and Computing, 17, 1, doi: [10.1016/j.ascom.2016.05.006](https://doi.org/10.1016/j.ascom.2016.05.006)

Hatzes, A. P., Gandolfi, D., Korth, J., et al. 2022, AJ, 163, 223, doi: [10.3847/1538-3881/ac5dcdb](https://doi.org/10.3847/1538-3881/ac5dcdb)

Herman, M. K., Zhu, W., & Wu, Y. 2019, AJ, 157, 248, doi: [10.3847/1538-3881/ab1f70](https://doi.org/10.3847/1538-3881/ab1f70)

Howard, A., Marcy, G., Johnson, J. A., et al. 2011, in American Astronomical Society Meeting Abstracts, Vol. 217, American Astronomical Society Meeting Abstracts #217, 415.06

Huang, C. X., Burt, J., Vanderburg, A., et al. 2018, ApJL, 868, L39, doi: [10.3847/2041-8213/aaef91](https://doi.org/10.3847/2041-8213/aaef91)

Huang, P., Yu, F., Lee, E. J., Dong, R., & Bai, X.-N. 2025, ApJ, 988, 94, doi: [10.3847/1538-4357/add11f](https://doi.org/10.3847/1538-4357/add11f)

Jenkins, J. M., Twicken, J. D., McCauliff, S., et al. 2016, in Software and Cyberinfrastructure for Astronomy IV, ed. G. Chiozzi & J. C. Guzman, Vol. 9913, International Society for Optics and Photonics (SPIE), 99133E, doi: [10.1117/12.2233418](https://doi.org/10.1117/12.2233418)

Jones, H. R. A., Paul Butler, R., Tinney, C. G., et al. 2002, MNRAS, 333, 871, doi: [10.1046/j.1365-8711.2002.05459.x](https://doi.org/10.1046/j.1365-8711.2002.05459.x)

Kipping, D. M. 2013, MNRAS, 435, 2152, doi: [10.1093/mnras/stt1435](https://doi.org/10.1093/mnras/stt1435)

Kovács, G., Zucker, S., & Mazeh, T. 2002, A&A, 391, 369, doi: [10.1051/0004-6361:20020802](https://doi.org/10.1051/0004-6361:20020802)

Kreidberg, L. 2015, PASP, 127, 1161, doi: [10.1086/683602](https://doi.org/10.1086/683602)

Kunimoto, M., Bryson, S., Jaffee, D., et al. 2025, AJ, 170, 280, doi: [10.3847/1538-3881/ae070a](https://doi.org/10.3847/1538-3881/ae070a)

Lefèvre-Forján, E., & Mulders, G. D. 2025, ApJ, 988, 101, doi: [10.3847/1538-4357/ade715](https://doi.org/10.3847/1538-4357/ade715)

Lightkurve Collaboration, Cardoso, J. V. d. M., Hedges, C., et al. 2018, Lightkurve: Kepler and TESS time series analysis in Python, Astrophysics Source Code Library, <http://ascl.net/1812.013>

Lissauer, J. J., Fabrycky, D. C., Ford, E. B., et al. 2011, Nature, 470, 53, doi: [10.1038/nature09760](https://doi.org/10.1038/nature09760)

Lubin, J., Van Zandt, J., Holcomb, R., et al. 2022, AJ, 163, 101, doi: [10.3847/1538-3881/ac3d38](https://doi.org/10.3847/1538-3881/ac3d38)

Mandel, K., & Agol, E. 2002, *The Astrophysical Journal*, 580, L171, doi: [10.1086/345520](https://doi.org/10.1086/345520)

Masuda, K., Winn, J. N., & Kawahara, H. 2020, *AJ*, 159, 38, doi: [10.3847/1538-3881/ab5c1d](https://doi.org/10.3847/1538-3881/ab5c1d)

Mayor, M., Marmier, M., Lovis, C., et al. 2011, arXiv e-prints, arXiv:1109.2497, doi: [10.48550/arXiv.1109.2497](https://doi.org/10.48550/arXiv.1109.2497)

Motalebi, F., Udry, S., Gillon, M., et al. 2015, *A&A*, 584, A72, doi: [10.1051/0004-6361/201526822](https://doi.org/10.1051/0004-6361/201526822)

Owen, J. E., & Wu, Y. 2017, *ApJ*, 847, 29, doi: [10.3847/1538-4357/aa890a](https://doi.org/10.3847/1538-4357/aa890a)

Perrier, C., Sivan, J.-P., Naef, D., et al. 2003, *A&A*, 410, 1039, doi: [10.1051/0004-6361:20031340](https://doi.org/10.1051/0004-6361:20031340)

Petigura, E. A., Marcy, G. W., Winn, J. N., et al. 2018, *AJ*, 155, 89, doi: [10.3847/1538-3881/aaa54c](https://doi.org/10.3847/1538-3881/aaa54c)

Philipot, F., Lagrange, A.-M., Kiefer, F., et al. 2023, *A&A*, 678, A107, doi: [10.1051/0004-6361/202346612](https://doi.org/10.1051/0004-6361/202346612)

Pont, F., Zucker, S., & Queloz, D. 2006, *MNRAS*, 373, 231, doi: [10.1111/j.1365-2966.2006.11012.x](https://doi.org/10.1111/j.1365-2966.2006.11012.x)

Ricker, G. R., Winn, J. N., Vanderspek, R., et al. 2015, *Journal of Astronomical Telescopes, Instruments, and Systems*, 1, 014003, doi: [10.1117/1.JATIS.1.1.014003](https://doi.org/10.1117/1.JATIS.1.1.014003)

Rosenthal, L. J., Fulton, B. J., Hirsch, L. A., et al. 2021, *ApJS*, 255, 8, doi: [10.3847/1538-4365/abe23c](https://doi.org/10.3847/1538-4365/abe23c)

Rosenthal, L. J., Knutson, H. A., Chachan, Y., et al. 2022, *ApJS*, 262, 1, doi: [10.3847/1538-4365/ac7230](https://doi.org/10.3847/1538-4365/ac7230)

Santerne, A., Malavolta, L., Kosiarek, M. R., et al. 2019, arXiv e-prints, arXiv:1911.07355, doi: [10.48550/arXiv.1911.07355](https://doi.org/10.48550/arXiv.1911.07355)

Santos, N. C., Israeli, G., & Mayor, M. 2001, *A&A*, 373, 1019, doi: [10.1051/0004-6361:20010648](https://doi.org/10.1051/0004-6361:20010648)

—. 2004, *A&A*, 415, 1153, doi: [10.1051/0004-6361:20034469](https://doi.org/10.1051/0004-6361:20034469)

Schlecker, M., Mordasini, C., Emsenhuber, A., et al. 2021, *A&A*, 656, A71, doi: [10.1051/0004-6361/202038554](https://doi.org/10.1051/0004-6361/202038554)

Stassun, K. G., Oelkers, R. J., Paegert, M., et al. 2019, *The Astronomical Journal*, 158, 138, doi: [10.3847/1538-3881/ab3467](https://doi.org/10.3847/1538-3881/ab3467)

Teske, J., Díaz, M. R., Luque, R., et al. 2020, *AJ*, 160, 96, doi: [10.3847/1538-3881/ab9f95](https://doi.org/10.3847/1538-3881/ab9f95)

Van Zandt, J., Petigura, E. A., Lubin, J., et al. 2025, *AJ*, 169, 235, doi: [10.3847/1538-3881/adbbed](https://doi.org/10.3847/1538-3881/adbbed)

Vogt, S. S., Burt, J., Meschiari, S., et al. 2015, *ApJ*, 814, 12, doi: [10.1088/0004-637X/814/1/12](https://doi.org/10.1088/0004-637X/814/1/12)

Wright, J. T., Marcy, G. W., Howard, A. W., et al. 2012, *ApJ*, 753, 160, doi: [10.1088/0004-637X/753/2/160](https://doi.org/10.1088/0004-637X/753/2/160)

Xiao, G.-Y., Liu, Y.-J., Teng, H.-Y., et al. 2023, *Research in Astronomy and Astrophysics*, 23, 055022, doi: [10.1088/1674-4527/accb7e](https://doi.org/10.1088/1674-4527/accb7e)

Xuan, J. W., & Wyatt, M. C. 2020, *MNRAS*, 497, 2096, doi: [10.1093/mnras/staa2033](https://doi.org/10.1093/mnras/staa2033)

Zhu, W. 2019, *ApJ*, 873, 8, doi: [10.3847/1538-4357/ab0205](https://doi.org/10.3847/1538-4357/ab0205)

—. 2024, *Research in Astronomy and Astrophysics*, 24, 045013, doi: [10.1088/1674-4527/ad3132](https://doi.org/10.1088/1674-4527/ad3132)

Zhu, W., & Dong, S. 2021, *ARA&A*, 59, 291, doi: [10.1146/annurev-astro-112420-020055](https://doi.org/10.1146/annurev-astro-112420-020055)

Zhu, W., Petrovich, C., Wu, Y., Dong, S., & Xie, J. 2018, *ApJ*, 860, 101, doi: [10.3847/1538-4357/aac6d5](https://doi.org/10.3847/1538-4357/aac6d5)

Zhu, W., & Wu, Y. 2018, *AJ*, 156, 92, doi: [10.3847/1538-3881/aad22a](https://doi.org/10.3847/1538-3881/aad22a)